Supporting Information

How Does a Surface Coating Dictate Bulk Structural Evolution in Spinel Cathodes?

Jiayong Chen[a,b], Xiaoxia Yang*[,b,c], Qin Wang[b,d], Junda Li[a,b], Xinyue Zhai[b], Guanjie Yan[e], Chunliu Li[e], Bo Wang[f], Zhongzhu Liu[f], Luanna Silveira Parreira[g], Robson S. Monteiro[g], Mingtao Li[b], Yuxin Zhao*[,h], Hao Liu*[,i], Laijun Liu*[,a] and Weibo Hua*[,b]

a. *School of Materials Science and Engineering, Guilin University of Technology, Guilin 541004, China. Email: ljliu2@163.com.*

b. *School of Chemical Engineering and Technology, State Key Laboratory of Electrical Insulation and Power Equipment, School of Instrument Science and Technology, Xi'an Jiaotong University, No.28, West Xianning Road, Xi'an 710049, China. Email: weibo.hua@xjtu.edu.cn.*

c. *School of Energy and Materials Engineering, Taiyuan University of Science and Technology, No. 66, Waliu Road, Taiyuan 030024, China. E-mail: yangxiaoxia1@tyust.edu.cn.*

d. *School of Chemical Engineering, Sichuan University, No. 24 South Section 1, Yihuan Road, Chengdu 610065, China.*

e. *South Manganese Group Limited, No. 18 Zhujin Road, Nanning 530028, China.*

f. *Capital Mansion, No.6 Xinyuan South Road, Chaoyang District, CITIC Metal Co. Ltd, Beijing 100027, China.*

g. *Companhia Brasileira de Metalurgia e Mineração (CBMM), Araxá, Minas Gerais 38183-903, Brazil.*

h. *The State Key Laboratory of Service Behavior and Structural Safety of Petroleum Pipe and Equipment Materials, CNPC Tubular Goods Research Institute (TGRI), Xi'an 710077, P. R. China. Email: zhaoyuxin1@yeah.net.*

i. *Institute for Applied Materials (IAM), Karlsruhe Institute of Technology (KIT), Hermann-von-Helmholtz-Platz 1, Eggenstein-Leopoldshafen, 76344, Karlsruhe. Germany. Email: yierliuhao@163.com.*

1. Experimental section

1.1 Material preparation

$LiMn_2O_4$ was prepared by a conventional solid-state reaction. Specifically, the stoichiometric Li_2CO_3 and Mn_3O_4 were well mixed followed by preheating at 500 °C for 6 h and subsequent calcination at 850 °C for 12 h in air to obtain pure LMO.

$LiNbO_3$-coated $LiMn_2O_4$ ($LiNbO_3$@LMO) was synthesized via a combined solid-state and precipitation-assisted route. For surface modification, the as-prepared LMO was dispersed into the deionized water under continuous stirring. Subsequently, an aqueous NaOH solution and ammonium niobate oxalate solution were slowly added dropwise into the LMO suspension. The temperature and pH of reaction system were precisely controlled at 45 °C and 11.0 ± 0.05, enabling the controlled precipitation of niobium-containing species onto the LMO surface. The precipitation was collected by filtration with deionized water, and dried at 100 °C overnight. Finally, the obtained precursor was mixed with a stoichiometric amount of $LiOH·H_2O$ followed by calcination at 600 °C for 5 h in air to obtain the $LiNbO_3$@LMO composite.

1.2. Material Characterization

The crystal structures of the as-synthesized samples were examined by powder X-ray diffraction (XRD) using a LaB-X diffractometer with Cu Kα radiation (λ = 1.5418 Å). Diffraction patterns were collected within a 2θ range of 10-70° with a scanning rate of 10° min^{-1}. Rietveld refinement was performed using the FullProf software package to obtain accurate lattice parameters.

Temperature-dependent Raman spectroscopy was conducted using a DEEP-INRS-II Raman characterization system to investigate the thermal evolution of niobium oxide species on the cathode surface. Atomic pair distribution function (PDF) measurements were carried out at the SPring-8 synchrotron radiation facility (Japan) to probe the local atomic structure of LMO and $LiNbO_3$@LMO samples.

The particle morphology of the samples was examined by scanning electron microscopy (SEM, MAIA3 LMH). The microstructure and elemental distribution were further analyzed by high-resolution transmission electron microscopy (HRTEM, Thermo Fisher Talos F200X).

In situ X-ray diffraction measurements were performed using a DEEP-XRD-R system to monitor the structural evolution of the samples during lithiation and delithiation. The collected in situ XRD patterns were further analyzed by Rietveld refinement using the FullProf software to track the evolutions of the lattice parameters

as a function of electrochemical state.

1.3. Electrochemical measurements

The electrochemical performance of LMO and $LiNbO_3$@LMO was evaluated by galvanostatic charge-discharge measurements using CR2032 coin cells. The cathode was prepared by mixing active material (LMO or $LiNbO_3$@LMO), super-P conductive agent, and polyvinylidene fluoride (PVDF) at a mass ratio of 8:1:1, and then was dissolved in N-methyl-2-pyrrolidone (NMP) followed by coating, drying and cutting into circular discs with a diameter of 1.2 cm. The separator was a Celgard 2400 membrane, lithium metal as the anode. The electrolyte comprises a mixture of $LiPF_6$ (1 M) with ethylene carbonate (EC) and dimethyl carbonate (DMC) in a 1:1 (volume ratio). The active material mass loading was approximately 5-6 mg cm^{-2}. The cell assembly was performed in a glove box within argon atmosphere. Electrochemical testing was conducted on a Neware tester within a voltage range from 3.0 to 4.3 V (vs. Li^+/Li) at 25 ℃. Electrochemical impedance spectroscopy (EIS) analysis at the frequency ranging from 100 kHz to 0.1 Hz with an amplitude of ±10 mV and cyclic voltammetry (CV) were performed on an electrochemical workstation (CHI660E, Chenhua) with a voltage range of 3.0-4.3 V.

The Galvanostatic Intermittent Titration Technique (GITT) was applied to evaluate the Li^+ transport kinetics during charge and discharge. A current pulse of 16 mA g^{-1} was applied for 20 min (τ), followed by a relaxation of 3 h period to reach a quasi-equilibrium state. This sequence was repeated iteratively across the voltage range of 3.0-4.3 V. The Li^+ diffusion coefficient (D_{Li+}) was calculated using the following equation:

$$D_{Li+} = \frac{4}{\pi\tau}\left(\frac{m_B V_M}{M_B S}\right)^2\left(\frac{\Delta E_s}{\Delta E_\tau}\right)^2 \left(\tau \ll \frac{L^2}{D}\right)\{\text{Ding, 2022 \#2793}\}$$

Where, τ is the duration of the applied current pulse; m_B is the mass of the active material; V_m and M_B are the molar volume and molecular weight of the electrode material, respectively; S denotes the active surface area of the electrode-electrolyte interface; ΔE_S represents the steady-state voltage change after relaxation; $\Delta E\tau$ is the transient voltage change during the current pulse; and L represents the Li^+ diffusion length from the lattice to the electrolyte.

2. Additional results

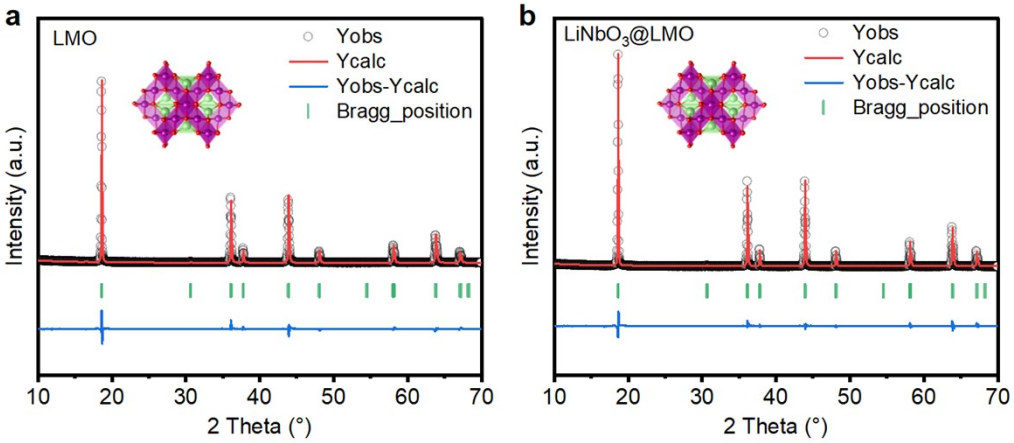

Figure S1. XRD patterns and corresponding Rietveld refinement results of (a) LMO and (b) $LiNbO_3$@LMO.

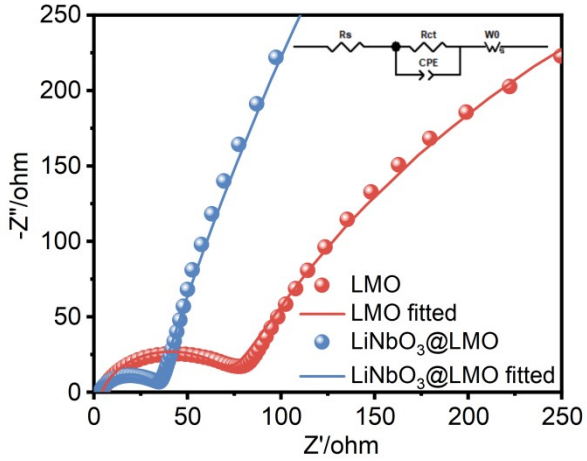

Figure S2. Nyquist plots of LMO and $LiNbO_3$@LMO, with the equivalent circuit inset.

The Li^+ transport kinetics of LMO and $LiNbO_3$@LMO were analyzed via electrochemical impedance spectroscopy (EIS). As shown in **Figure S2**, **S6** and **S8**, the EIS curves of both electrodes comprise semicircle in the high-to-mid frequency range and sloping line in the low-frequency region. Inset presents the corresponding equivalent circuit. Series resistance (R_s), mainly originating from the electrolyte, current collector, and electrode/electrolyte interface contact, reflects the overall ohmic resistance of the cell. The semicircle in the high-frequency region corresponds to the charge transfer resistance (R_{ct}), while the sloping segment in the low-frequency region is identified as the Warburg resistance (W_o). The lithium-ion diffusion coefficients for LMO and $LiNbO_3$@LMO are calculated using the following equations:

$$D_{Li^+} = \frac{R^2T^2}{2n^4F^4A^2\sigma^2c^2}$$

Where, D represents the Li^+ diffusion coefficient; R is the universal gas constant; T denotes the absolute temperature; n corresponds to the number of electrons transferred per molecule in the electrochemical reaction; F is the Faraday constant; A is the electrode surface area; σ is the Warburg impedance parameter; and c refers to the molar concentration of Li^+.

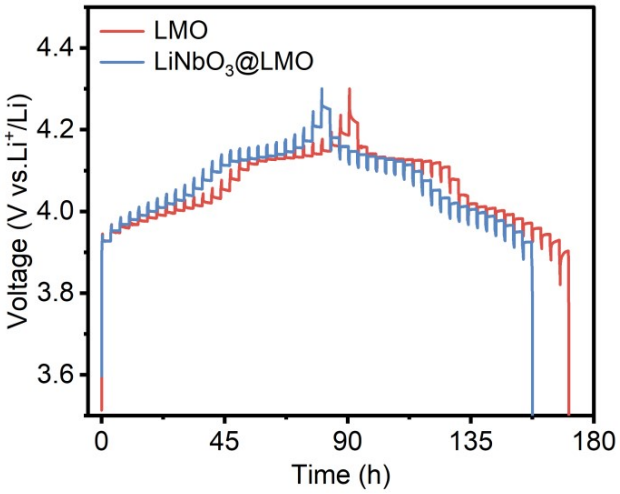

Figure S3. GITT curves of LMO and $LiNbO_3$@LMO cathodes during the second charge/discharge process.

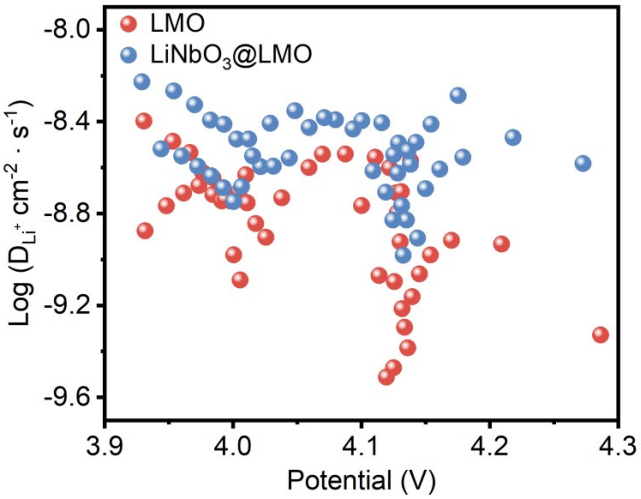

Figure S4. Li^+ diffusion coefficients derived from GITT measurements as a function of potential for LMO and $LiNbO_3$@LMO electrodes.

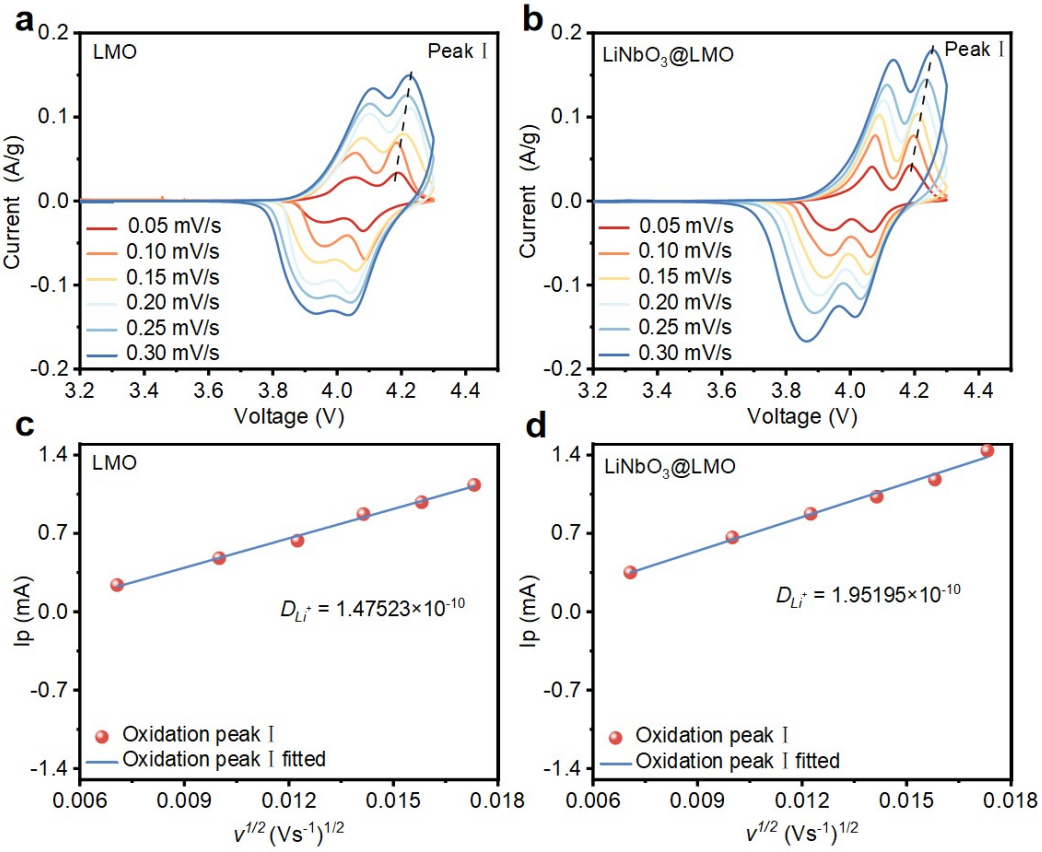

Figure S5. Cyclic voltammetry (CV) curves of (a) LMO and (b) $LiNbO_3$@LMO recorded at different scanning rates, and the corresponding fitted Li^+ diffusion plots of (c) LMO and (d) $LiNbO_3$@LMO.

The linear relationship between the peak current density and the square root of the scan rate is presented in **Figure S5c** and **S5d**. The lithium-ion diffusion coefficient (D_{Li+}) of the samples can be calculated based on the Randles-Sevick equation (Eq):

$$I_p = 2.686 \times 10^5 \times n^{3/2} C A D_{Li^+}{}^{1/2} v^{1/2}$$

Where, I_p denotes the peak current; n is the number of electrons involved in the redox process ($n \approx 1$ for $LiMn_2O_4$); C represents the bulk Li^+ concentration in the cathode (0.0237 mol cm^{-3}); A corresponds to the effective electrode surface area; and v is the scan rate expressed in mV s^{-1}.

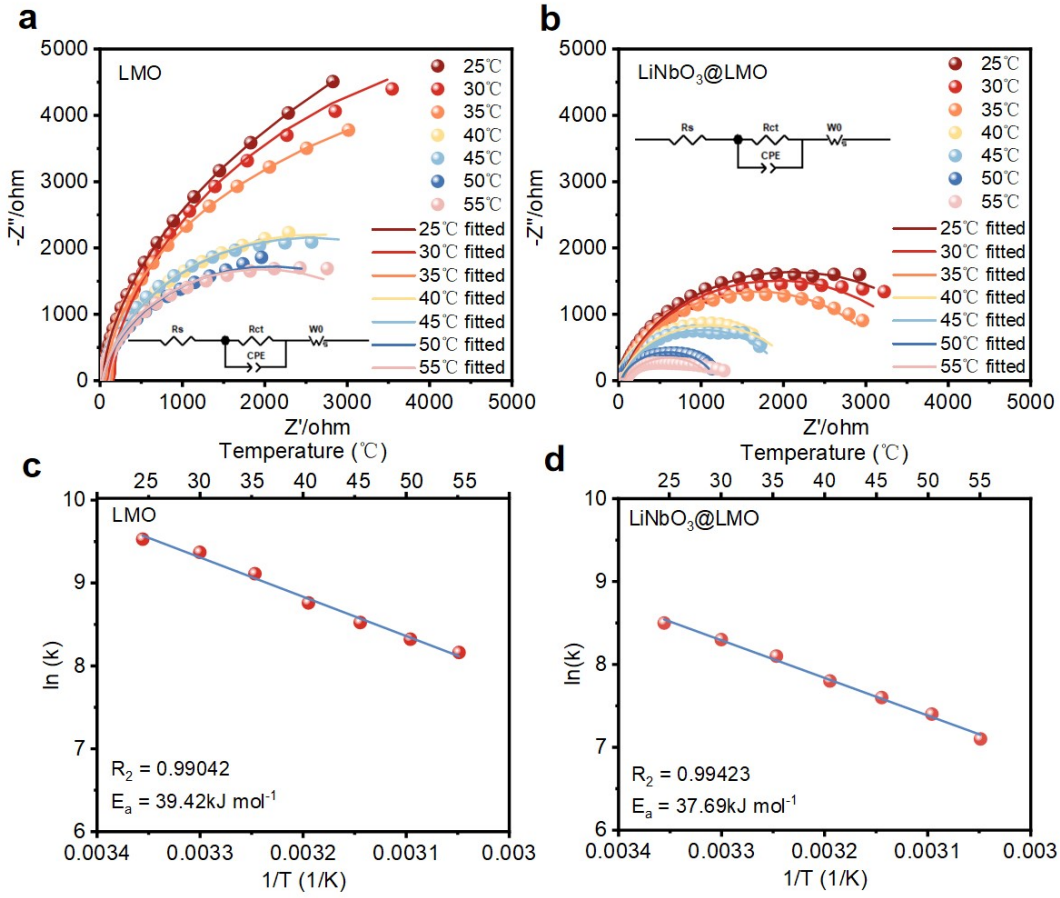

Figure S6. EIS of (a) LMO and (b) $LiNbO_3$@LMO measured at different temperatures, and the corresponding Arrhenius plots for the determination of activation energies of (c) LMO and (d) $LiNbO_3$@LMO.

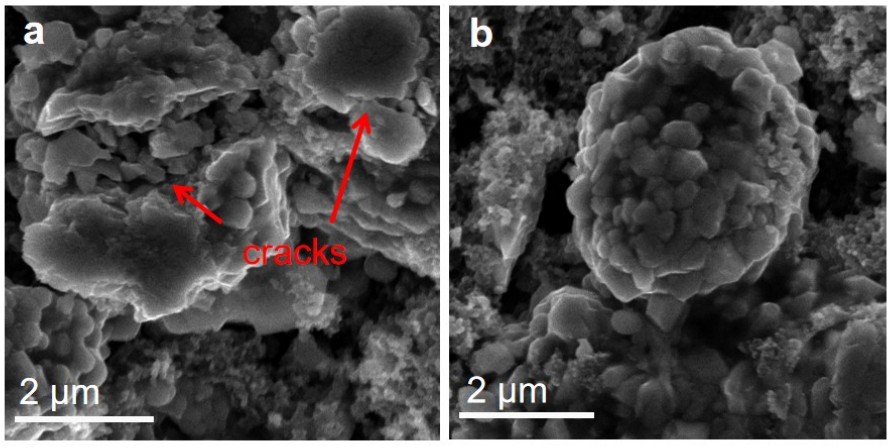

Figure S7. SEM images of (a) LMO and (b) $LiNbO_3$@LMO after cycling.

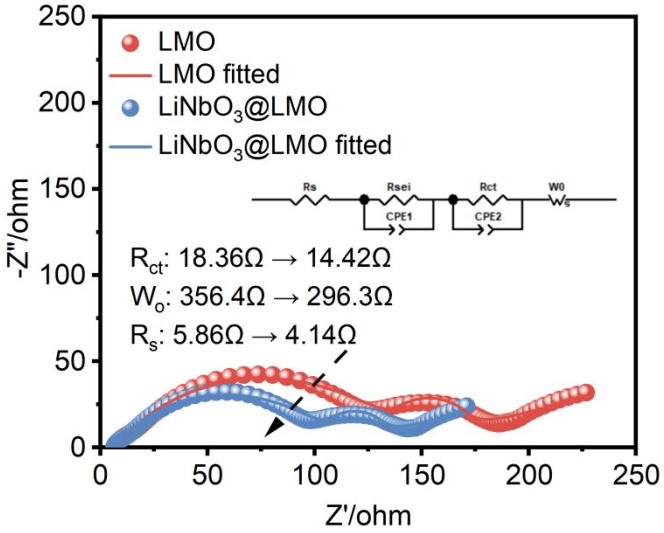

Figure S8. Nyquist plots of LMO and $LiNbO_3$@LMO electrodes after cycling, along with the corresponding fitted curves; the inset shows the equivalent circuit model.

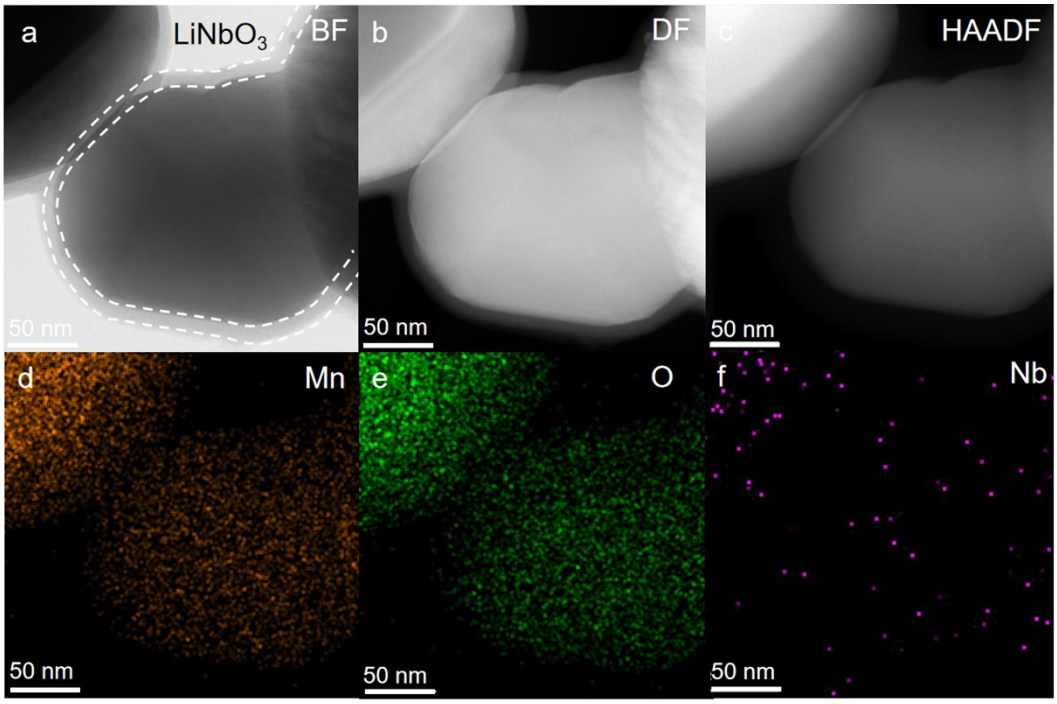

Figure S9. Microstructure of $LiNbO_3$@LMO. (a) BF-TEM image; (b) DF-TEM images; (c) HAADF-TEM images; (d-f) EDS element mapping profile of $LiNbO_3$@LMO.

Table S1. Crystallographic parameters of LMO.

Note: Fract is the fractional occupancy of the atom on this site.

Cell parameters

Space group: $Fd\bar{3}m$, a = 8.243981 (5) Å, b = 8.243981 (5) Å, c = 8.243981 (5) Å, gamma = 90°, V = 560.288 (6) Å^3,

Atomic positions

Name	site	*x*	*y*	*z*	Fract
Li1	8*a*	0.125	0.125	0.125	1.000
Mn1	16*d*	0.500	0.500	0.500	1.000
O1	32*e*	0.263	0.263	0.263	1.000

Refinement parameters

R_{wp}= 4.95%, R_p= 5.75%, χ^2: 9.39

Table S2. Crystallographic parameters of $LiNbO_3$@LMO.
Note: Fract is the fractional occupancy of the atom on this site.

Cell parameters

Space group: $Fd\bar{3}m$, a = 8.239970 (4) Å, b = 8.239970 (4) Å, c = 8.239970 (4) Å, gamma = 90°, V = 559.470 (5) Å^3,

Atomic positions

Name	site	x	y	z	Fract
Li1	8*a*	0.125	0.125	0.125	1.000
Mn1	16*d*	0.500	0.500	0.500	1.000
O1	32*e*	0.261	0.261	0.261	1.000

Refinement parameters

R_{wp}= 4.13%, R_p= 5.18%, χ^2: 8.55

Table S3. Comparison of the first-cycle discharge specific capacity and specific capacity fade between $LiNbO_3$@LMO and other LMO lithium manganate cathode materials.

Molecular formula	Work environment (V, ℃)	First-cycle electrochemical performance	Capacity decay (mAh g^{-1}/cycle)	References
LMO@2%LAO	3.0-4.3, 25	104.63 mAh g^{-1} at 1 C	0.052	[24]
2%LBO@LMO	3.0-4.3, 25	117 mAh g^{-1} at 1 C	0.045	[27]
LMO-MA1	3.0-4.3, 25	127.89 mAh g^{-1} at 1 C	0.070	[28]
AZLMO-3	3.0-4.3, 25	109.2 mAh g^{-1} at 1 C	0.019	[29]
NTO-LMO	3.0-4.3, 25	112.7 mAh g^{-1} at 1 C	0.043	[30]
3%ALP@LMO	3.3-4.3, 25	124.2 mAh g^{-1} at 1 C	0.075	[31]
Sm-LMO	3.0-4.3，25	102.9 mAh g^{-1} at 1 C	0.036	[32]
LMO@NCM1%	3.0-4.3, 25	119.74 mAh g^{-1} at 1 C	0.046	[33]
$LiNbO_3$@LMO	3.0-4.3, 25	117 mAh g^{-1} at 1 C	0.025	This work